Front. Chem. Sci. Eng. 2019, 13(2): 324–329
https://doi.org/10.1007/s11705-019-1792-5

COMMUNICATION

# Molecular dynamics simulations of initial Pd and PdO nanocluster growth in a magnetron gas aggregation source

**Pascal Brault (✉)[1], William Chamorro-Coral[1], Sotheara Chuon[1], Amaël Caillard[1], Jean-Marc Bauchire[1], Stève Baranton[2], Christophe Coutanceau[2], Erik Neyts[3]**

1 GREMI UMR 7344 CNRS, Université d'Orléans, 45067 Orléans Cedex 2, France
2 IC2MP UMR 7285 CNRS, Université de Poitiers, 86073 Poitiers Cedex 9, France
3 Department of Chemistry, University of Antwerp, 2610 Antwerp, Belgium



**Abstract** Molecular dynamics simulations are carried out for describing growth of Pd and PdO nanoclusters using the ReaxFF force field. The resulting nanocluster structures are successfully compared to those of nanoclusters experimentally grown in a gas aggregation source. The PdO structure is quasi-crystalline as revealed by high resolution transmission microscope analysis for experimental PdO nanoclusters. The role of the nanocluster temperature in the molecular dynamics simulated growth is highlighted.

**Keywords** molecular dynamics, cluster growth, plasma sputtering, nanocatalyst

## 1 Introduction

Nanoparticles (NPs) play a central role in many applications. Among them catalysis represents certainly a broad field of uses [1]. The open questions are centered on the capability of producing nanoclusters with well-defined size and shape distributions. Physical vapor deposition (PVD) techniques are now mature synthesis methods able to reach such goals [2]. Among all possible PVD techniques, the magnetron gas aggregation is rapidly becoming a widely used technique due to its simplicity and its convenience to allow the growth of a large kind of metallic and metal-oxide nanoparticles [3–18]. Despite numerous studies on particle growth, either experimental or theoretical/numerical as reviewed in Ref. 18, very few of them take into account the reactivity at the molecular level under conditions matching those of experimental synthesis of NPs.

Received July 26, 2018; accepted October 27, 2018

E-mail: pascal.brault@univ-orleans.fr

Molecular dynamics simulation (MDs) is a very efficient technique for describing atomic and molecular processes, especially at the nanoscale. It consists in solving the Newton equations of motion (or Langevin dynamics which includes energy dissipation through an additional friction term):

$$\frac{\partial^2}{\partial t^2}\vec{r}_1 = \frac{1}{m_i}\vec{f}_{\mathrm{i}},\ \vec{f}_{\mathrm{i}} = -\frac{\partial}{\partial r}V\left(\vec{r}_1(t),\vec{r}_2(t),\cdots,\vec{r}_{\mathrm{N}}(t)\right), \quad (1)$$

where $\vec{r}_{\mathrm{i}}(t)$ is the position of the atom i belonging to an assembly of N atoms, at a time $t$ and with a mass $m_{\mathrm{i}}$, and $V$ is the interaction potential between all atoms. So solving such a set of equations requires the knowledge of the interaction potentials $V$ and a set of initial conditions, preferably matching experimental situations [19,20]. Moreover, recent developments now enable MD to treat molecular reactions allowing a direct comparison with experiments. This means that bond formation and bond breaking can be described. A widely used force field for achieving this goal is ReaxFF, which also includes variable partial charges allowing to study reactivity in ionic systems [21]. Additionally, both these force fields are including variable partial charges, increasing their interest in studying reactivity of ionic systems.

Palladium and palladium oxide NPs are of very high interest for catalytic combustion [22,23] and more recently for the conversion of biomass molecules into hydrogen and added-value compounds [24–27]. In this context, the present study examines the MDs of the growth of Pd and PdO NPs in conditions matching those of the gas aggregation source (GAS) setup. The theoretical structures of Pd and PdO NPs as calculated using MDs are compared with those determined from high resolution transmission electron microscopy pictures of experimentally grown PdO using a GAS setup.

## 2 Methods

The GAS setup (MANTIS Deposition Ltd.) was previously fully described in [6]. The scheme of Fig. 1 represents the working principle of the GAS. Pd atoms are sputtered from a Pd target (Lesker, 99.99% purity in a condensation chamber filled by a mixture of argon gas at a pressure of 38 Pa and a 100 sccm flow rate, and oxygen gas at a flow rate of 5 sccm. Magnetron sputtering is ignited by electrical breakdown of the Pd target biased at negative voltage $V_b = -400$ V. Growth of Pd and PdO clusters occurs in the condensation chamber and the clusters are leaving the condensation chamber via an outlet orifice with a diameter of 5 mm towards a differentially pumped deposition chamber. The nanoclusters are collected onto carbon-coated Cu grids (300 mesh, SPI) and analyzed on high resolution transmission microscope (HRTEM) JEM-ARM 200F Cold FEG TEM/STEM operating at 200 kV and equipped with a spherical aberration (Cs) probe and image correctors (point resolution 0.12 nm in TEM mode).

Molecular dynamics simulations of cluster growth are carried out using PdO ReaxFF potentials [28]. Ar-Pd and Ar-O interactions are described using Molière potentials [29]. The simulation box is representative of the GAS conditions, i.e., Ar pressure and flow rates of 30 Pa and 100 sccm respectively. Oxygen partial pressure and flowrate are 1.4 Pa and 1 sccm, respectively. Discharge current is 0.22 A while the target voltage is 430 V. The Pd to Ar, and O to Ar ratios are estimated using the procedure described by Quesnel et al. [9]. This leads to a simulation box containing 20000 Ar atoms, 500 Pd atoms and 0 to 1000 O atoms. The initial temperature of this vapor is $T_{gas} = 300$ K. Initial velocities of atoms are sampled from a Maxwell-Boltzmann distribution at 300 K. Moreover, while all calculations are performed considering a constant number of atoms, constant volume and constant total energy ensemble, while using NVT ensemble (Temperature is constant instead of E) for the Ar atoms, mimicking cluster cooling via Ar collisions on clusters and transport to chamber wall. Atoms are initially randomly located in a periodic simulation box of 40 nm × 40 nm × 40 nm. These initial values are deduced from the actual conditions used for the experimental cluster growth processes in the GAS setup. This follow the procedure described in Ref. 30. It is expected that they allow a relevant comparison with HRTEM observations of real clusters. The simulations are continued up to a simulated time of 25 ns, corresponding to $1.00 \times 10^8$ time-steps (the integration time-step is fixed to 0.25 fs, according to Ref. 28). All simulations are carried out using the LAMMPS software [31].

## 3 Results and discussion

Figure 2 displays snapshots of Pd growth at 25 ns elapsed calculation time in the absence (Fig. 2(a)) and in the presence (Fig. 2(b)) of oxygen. Ar atoms are not represented for clarity.

In the case of the formation of Pd clusters (Fig. 2(a)), no isolated Pd atoms remains after 25 ns: All Pd atoms are incorporated in the formed clusters. Four clusters are present, containing 286, 159, 45 and 10 atoms. Indeed, considering the boundary conditions, the two pseudo-clusters visible close to the bottom of Fig. 2(a) belong to the same cluster. According to the radial distribution function (RDF) plot in Fig. 3, the Pd clusters appear well organized and crystalline. The interatomic distances between a Pd atom and the four nearest neighbor atoms (NNA) determined from the RDF plot are very close to the theoretical ones for Pd bulk (Table 1), which confirms the crystalline nature of the Pd clusters obtained by MD simulations.

Another important point concerns the Pd vapor-cluster temperature change during the cluster growth. Figure 4 displays the change in temperature of the Pd (red curve) and $PdO_x$ (black curve) vapor-cluster for 25 ns of the MD simulations. In the case of Pd clusters, the temperature first increases during the growth of initial clusters. This temperature is controlled by the Pd sticking while the Pd dimer, trimer, …, NPs bond formation energy is removed partly by Ar atoms acting as a third body collision partner and partly by storing the remaining part of this bond energy

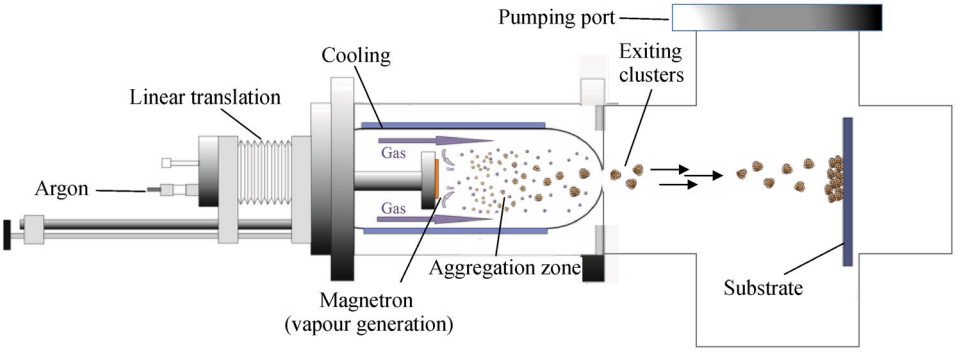


**Fig. 1** Scheme of the working principle of the gas aggregation source setup

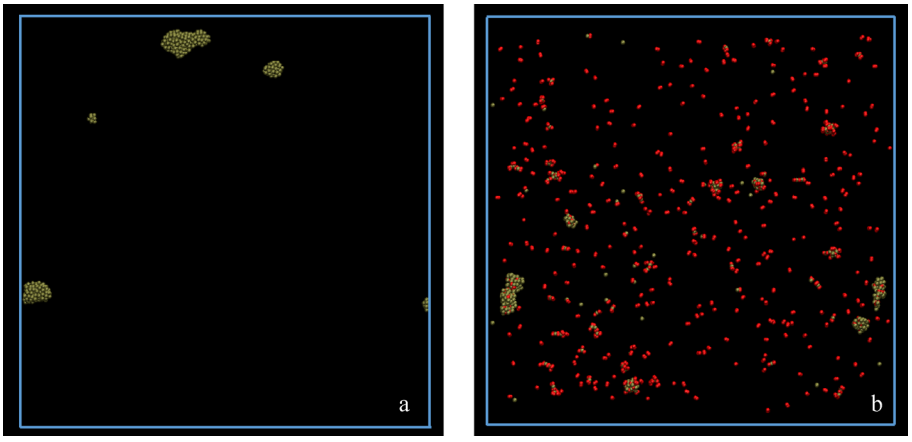


**Fig. 2** Snapshots at 25 ns calculation time for the growth of (a) Pd clusters considering 20000 Ar atoms (not shown for clarity), 500 Pd atoms and (b) $PdO_x$ considering 20000 Ar atoms (not shown for clarity), 500 Pd atoms and 500 $O_2$ molecules (right panel). Pd atoms are colored green and unreacted $O_2$ molecules are colored red

**Table 1** Interatomic distances between a Pd atom and the four NNA in Pd clusters determined from the RDF plot (Fig. 3) and theoretical ones in Pd bulk

| | Position/Å | | | |
|---|---|---|---|---|
| | 1st NNA | 2nd NNA | 3rd NNA | 4th NNA |
| Pd cluster | 2.75 | 4.05 | 4.70 | 5.50 |
| Pd bulk | 2.75 | 3.89 | 4.76 | 5.50 |

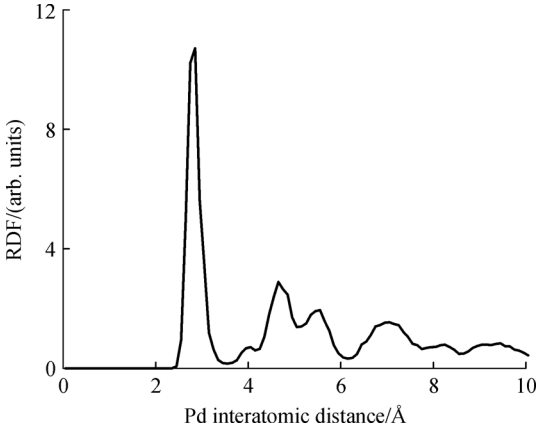


**Fig. 3** RDF plot of Pd nanoclusters of Fig. 2

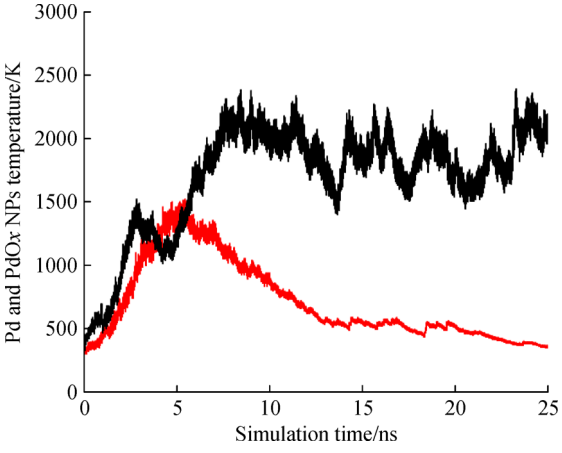


**Fig. 4** Pd vapor (red curve) and $Pd_xO_y$ in $Pd/O_2$ vapor (black curve) temperatures changes for the growth of Pd nanoclusters and $Pd_xO_y$ nanoclusters

in the molecule or NP itself as internal vibrational excitation. A maximum temperature is then reached when coalescence of atoms leads to clusters sufficiently big to be cooled by the argon collisions. Further, the cluster temperature decreases down to the argon temperature (300 K in the present case) while collisions and coalescence of clusters become rare events. Bumps after 15 ns correspond to the coalescences of two clusters. At 25 ns, the remaining Pd nanoclusters are fully thermalized.

When adding $O_2$ to the Ar sputtering gas, the cluster growth is affected in numerous ways. When looking at the snapshot in Fig. 2(b), Pd clusters are partly oxidized and do not appear well crystallized after 25 ns simulation time. Moreover 55% of the initial $O_2$ molecules are not inserted in or adsorbed on clusters, and remain at this step as unreacted molecules in the environmental atmosphere. The comparison of the snapshot for the formation of Pd clusters in the presence of $O_2$ molecules (Fig. 2(b)) with that for the formation of Pd clusters in the absence of $O_2$ molecules

(Fig. 2(a)) indicates clearly that the number of clusters is higher in the presence of $O_2$ molecules than in their absence. Non-negligible amounts of $PdO_x$ and $Pd_2O_x$ small molecules can also be seen. This indicates that the clustering process needs more time in the presence of dioxygen than without. This is confirmed by looking at the change of the temperature of the $Pd_xO_y$ species (non-bonded $O_2$ molecules are excluded from this temperature calculation) in Fig. 4 (black curve). As for the formation of Pd clusters, the temperature first increases due to the formation of Pd-Pd chemical bonds. This process is followed by a short decrease of the temperature at a time close to that for pure Pd clusters, indicating that Pd clusters are not so highly oxidized at this step. At longer times, an increase of temperature is observed, which is due to the formation of a significant amount of Pd-O bonds. The formation of such chemical bond releases a higher energy than that for the formation of a Pd-Pd chemical bond, i.e., about 1.3 eV for O adsorption on Pd and between 0.5 and 1 eV for Pd adsorption on Pd [28]. Afterwards, the temperature oscillates but does not decrease, despite the 20000 Ar atoms thermostating the $Pd_xO_y$ clusters and the remaining $O_2$ molecules. These oscillations of temperature are related to the collision and coalescence of smaller cluster into bigger ones. This means that longer computation time is necessary to obtain fully thermalized $Pd_xO_y$ clusters. On the other hand the cluster composition has not yet reached the stable PdO stoichiometric composition. The larger $Pd_xO_y$ clusters exhibit an O/Pd ratio of 0.25 to 0.3, while smaller clusters are rather molecules of the form $PdO_x$ and $Pd_2O_x$. This is also an indication that the clustering process is slower for $Pd_xO_y$ than for Pd for which, for the same computation time of 25 ns, no isolated Pd atom, dimers, trimers, etc., remains in the gas phase.

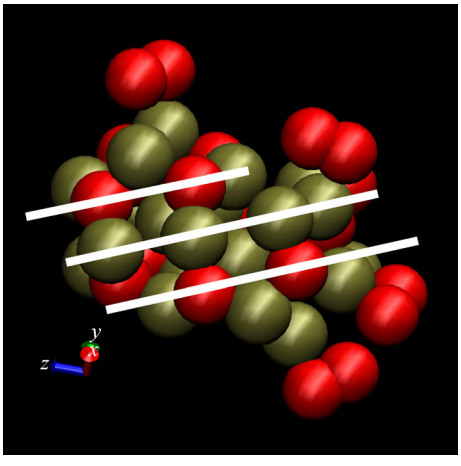


**Fig. 5** Snapshot of a $Pd_{21}O_{23}$ cluster issued from Fig. 2. White lines underline the nascent Pd-O alternate layers. $O_2$ molecules at the cluster edges are adsorbed molecules

Nevertheless, one of the clusters in Fig. 2(b) has a nearly stoichiometric composition of $Pd_{21}O_{23}$. Figure 5 depicts the atomic structure of this cluster. It is clearly observable that this cluster exhibits a nascent typical alternate Pd-O layered structure with the stoichiometry of pure PdO. This observation indicates that the formation of stoichiometric and crystalline PdO clusters can be expected for longer simulation times, i.e., when clusters will start to thermalize.

In order to compare the clusters obtained experimentally in the GAS set up experiments to those obtained from the MD simulations, which included starting conditions matching the experimental ones, HRTEM micrographs of a PdO experimental cluster were taken (Fig. 6(a)). The zoom in Fig. 6(b) and the selected area electron diffraction (SAED) pattern along the [010] axis (inset of Fig. 6(b)) reveal that we are in the presence of a PdO cluster. This is confirmed by the interplanar spacing of 0.266 and 0.156 nm and the angle between planes of around 30° corresponding to the {101} and {103} crystallographic planes of the PdO phase. In the micrograph it is also possible to observe the presence of 2D crystal defects as stacking faults and twin boundaries. The zoomed-in portion of the micrograph (Fig. 6(b)) shows clearly the position of the Pd atoms (oxygen are light atoms that are not detected) that matches the body centered tetragonal structure of PdO as shown in the schematic. The SAED

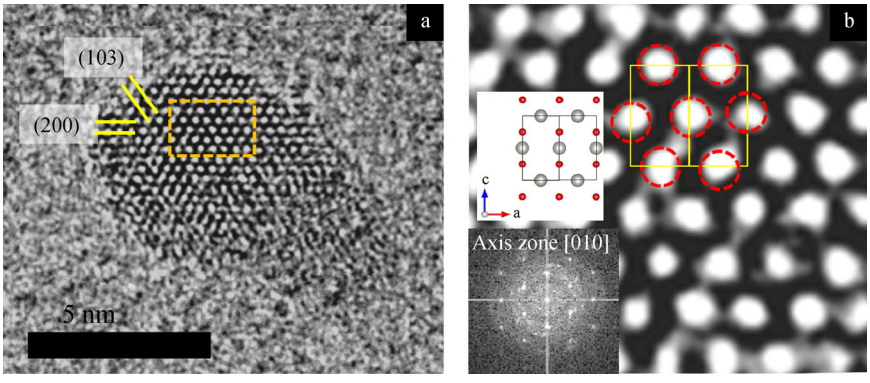


**Fig. 6** HRTEM micrograph showing (a) an isolated PdO cluster with a size of 7 nm and (b) zoom with a draw of the PdO crystal cell. Inset PdO SAED pattern along the [010] zone axis

pattern along the [010] zone axis shows a PdO crystal with a good crystal quality. The presence of oxygen introduces internal strains that deform the Pd crystal cell, as observed by the increase of the Pd-Pd interatomic distance (Table 1). Oxygen addition also increases the 2D defects due to the PdO formation.

Therefore, the structure of the experimentally obtained PdO nanoclusters using the GAS setup is partly in agreement with that foreseen using MD simulation based on initial conditions matching those of experimental synthesis: only a small amount of $PdO_x$ NPs are stoichiometric. This indicates clearly that MD simulation is a very powerful method to predict the growth mechanism and structure of metal and metal oxide nanoparticles.

## 4 Conclusions

Reactive molecular dynamics simulations are carried out for describing the initial steps of the formation of Pd and PdO nanoclusters under conditions mimicking those for the growth of clusters in a magnetron gas aggregation source setup. When the formation of Pd clusters is carried out in the absence of $O_2$, the clustering process is complete at 25 ns simulation time. When adding oxygen in the sputtering gas clustering process is incomplete and small molecules such as $PdO_x$ and $Pd_2O_x$ are numerous; moreover 55% of the $O_2$ molecules did not react. This leads to kinetics of $PdO_x$ cluster growth considerably slower than that of Pd cluster growth. Pd oxide NPs are observed with an O/Pd ratio close to 0.25–0.30. Nevertheless, stoichiometric PdO nanoclusters are also observed, which exhibit a nascent crystalline structure, while the cluster temperature of around 2000 K does not allow exhibiting a relaxed crystalline structure. On the other hand, experimental cluster formation in magnetron gas aggregation source setup performed under comparable experimental conditions as those used in the simulations leads to the observation by HRTEM of stoichiometric and crystalline PdO nanoclusters.

**Acknowledgements** Part of this work has been funded by French "Agence Nationale de la Recherche" under grant ANR-16-CE29-007.

## References

1. Tao F, Catalysis Series No R S C. 17, Metal Nanoparticles for Catalysis: Advances and Applications. Cambridge: Royal Society of Chemistry, 2014
2. Brault P. Review of low pressure plasma processing of proton exchange membrane fuel cell electrocatalysts. Plasma Processes and Polymers, 2016, 13: 10–18
3. Wegner K, Piseri P, Vahedi Tafreshi H, Milani P. Cluster beam deposition: A tool for nanoscale science and technology. Journal of Physics. D, Applied Physics, 2006, 39: R439–R459
4. Marek A, Valter J, Kadlec S, Vyskočil J. Gas aggregation nanocluster source—reactive sputter deposition of copper and titanium nanoclusters. Surface and Coatings Technology, 2011, 205: S573–S576
5. Ayesh A I. Production of metal-oxide nanoclusters using inert-gas condensation technique. Thin Solid Films, 2017, 636: 207–213
6. Caillard A, Cuynet S, Lecas T, Andreazza P, Mikikian M, Thomann A L, Brault P. PdPt catalyst synthesized using a gas aggregation source and magnetron sputtering for fuel cell electrodes. Journal of Physics. D, Applied Physics, 2015, 48: 475302
7. Kylián O, Valeš V, Polonskyi O, Pešička J, Čechvala J, Solař P, Choukourov A, Slavínská D, Biederman H. Deposition of Pt nanoclusters by means of gas aggregation cluster source. Materials Letters, 2012, 79: 229–231
8. Watanabe Y, Wu X, Hirata H, Isomura N. Size-dependent catalytic activity and geometries of size-selected Pt clusters on $TiO_2$(110) surfaces. Catalysis Science & Technology, 2011, 1: 1490–1495
9. Quesnel E, Pauliac-Vaujour E, Muffato V. Modeling metallic nanoparticle synthesis in a magnetron-based nanocluster source by gas condensation of a sputtered vapor. Journal of Applied Physics, 2010, 107: 054309
10. Ayesh A I, Thaker S, Qamhieh N, Ghamlouche H. Size-controlled Pd nanocluster grown by plasma gas-condensation method. Journal of Nanoparticle Research, 2011, 13: 1125–1131
11. Drabik M, Choukourov A, Artemenko A, Polonskyi O, Kylian O, Kousal J, Nichtova L, Cimrova V, Slavinska D, Biederman H. Structure and composition of titanium nanocluster films prepared by a gas aggregation cluster source. Journal of Physical Chemistry C, 2011, 115: 20937–20944
12. Gojdka B, Hrkac V, Strunskus T, Zaporojtchenko V, Kienle L, Faupel F. Study of cobalt clusters with very narrow size distribution deposited by high-rate cluster source. Nanotechnology, 2011, 22: 465704
13. Bouchat V, Feron O, Gallez B, Masereel B, Michiels C, Vander Borght T, Lucas S. Carbon nanoparticles synthesized by sputtering and gas condensation inside a nanocluster source of fixed dimension. Surface and Coatings Technology, 2011, 205: S577–S581
14. Ten Brink G H, Krishnan G, Kooi B J, Palasantzas G. Copper nanoparticle formation in a reducing gas environment. Journal of Applied Physics, 2014, 116: 104302
15. Koch S A, Palasantzas G, Vystavel T, De Hosson J Th M, Binns C, Louch S. Magnetic and structural properties of Co nanocluster thin films. Physical Review. B, 2005, 71: 085410
16. Spadaro M C, D'Addato S, Gasperi G, Benedetti F, Lueches P, Grillo V, Bertoni G, Valeri S. Morphology, structural properties and reducibility of size-selected $CeO_{2-l}$ nanoparticle films. Beilstein Journal of Nanotechnology, 2015, 6: 60–67
17. D'Addato S, Spadar M C, Luches P, Grillo V, Frabboni S, Valeri S, Ferretti A M, Capetti E, Ponti A. Controlled growth of Ni/NiO core–shell nanoparticles: Structure, morphology and tuning of magnetic properties. Applied Surface Science, 2014, 306: 2–6
18. Polonskyi O, Ahadi A M, Tilo P, Fujioka K, Abraham J W, Vasiliauskaite E, Hinz A, Strunskus T, Wolf S, Bonitz M, et al. Plasma based formation and deposition of metal and metal oxide

nanoparticles using a gas aggregation source. European Physical Journal D, 2018, 72: 93

19. Brault P, Neyts E. Molecular dynamics simulations of supported metal nanocatalyst formation by plasma sputtering. Catalysis Today, 2015, 256: 3–12
20. Neyts P, Brault P. Molecular dynamics simulations for plasma surface interactions. Plasma Processes and Polymers, 2017, 14: 1600145
21. Liang T, Shin Y K, Cheng Y T, Yilmaz D E, Vishnu K G, Verners O, Zou C, Phillpot S R, Sinnott S B, van Duin A C T. Reactive Potentials for advanced atomistic simulations. Annual Review of Materials Research, 2013, 43: 109–129
22. Hu W, Li G X, Chen J J, Huang F J, Wu Y, Yuan S D, Zhong L, Chen Y Q. Enhanced catalytic performance of a PdO catalyst prepared via a two-step method of *in situ* reduction-oxidation. Chemical Communications (Cambridge), 2017, 53: 6160–6163
23. Huang F, Chen J, Hu W, Li G, Wu Y, Yuan S, Zhong L, Chen Y. Pd or PdO: Catalytic active site of methane oxidation operated close to stoichiometric air-to-fuel for natural gas vehicles. Applied Catalysis B: Environmental, 2017, 219: 73–81
24. Liang X, Liu C J, Kuai P. Selective oxidation of glucose to gluconic acid over argon plasma reduced $Pd/Al_2O_3$. Green Chemistry, 2008, 10: 1318–1322
25. Simões M, Baranton S, Coutanceau C. Electrochemical valorization of glycerol. ChemSusChem, 2012, 5: 2106–2124
26. Zalineeva A, Padilla M, Martinez U, Serov A, Artyushkova K, Baranton S, Coutanceau C, Atanassov P B. Self-supported Pd-Bi catalysts for the electrooxidation of glycerol in alkaline media. Journal of the American Chemical Society, 2014, 136: 3937–3945
27. Song S, Wang K, Yan L, Brouzgouc A, Zhang Y, Wang Y, Tsiakaras P. Ceria promoted Pd/C catalysts for glucose electrooxidation in alkaline media. Applied Catalysis B: Environmental, 2015, 176-177: 233–239
28. Senftle T P, Meyer R J, Janik M J, van Duin A C T. Development of a ReaxFF potential for Pd/O and application to palladium oxide formation. Journal of Chemical Physics, 2013, 139: 044109
29. Graves D, Brault P. Molecular dynamics for low temperature plasma-surface interaction studies. Journal of Physics. D, Applied Physics, 2009, 42: 194011
30. Brault P. Multiscale molecular dynamics simulation of plasma processing: Application to plasma sputtering. Frontiers in Physics, 2018, 6: 59
31. Plimpton S. Fast parallel algorithms for short-range molecular dynamics. Journal of Computational Physics, 1995, 117: 1–19